Supplementary Material For

Novel Pseudo-Hexagonal Montmorillonite Model and Microsecond MD Simulations of Hydrate Formation in mixed clay sediments with surface defects

Fengyi Mi[1,2], Jiangtao Pang[1], Wei Li[1], Othonas A. Moultos[2], Fulong Ning[1,a)], Thijs J.H. Vlugt[2,a)]

[1]National Center for International Research on Deep Earth Drilling and Resource Development, Faculty of Engineering, China University of Geosciences, Wuhan, Hubei 430074, China

[2]Engineering Thermodynamics, Process & Energy Department, Faculty of Mechanical Engineering, Delft University of Technology, Leeghwaterstraat 39, Delft, 2628CB, the Netherlands

[a)]Authors to whom correspondence should be addressed. nflzx@cug.edu.cn, t.j.h.vlugt@tudelft.nl

Total number of pages: 19

Total number of figures: 18

Total number of tables: 3

Total number of videos: 2

Total number of files: 2

Contents of Supplementary Material

S1. Simulation details

S1.1 Simulation Models

Illite and montmorillonite minerals are the most abundant clay minerals in the hydrate-bearing sediments in the Shenhu area of the South China Sea.[1] The illite and montmorillonite unit cell was obtained by modifying the pyrophyllite unit cell taken from the United States Mineral Crystal Structure Database.[2] The molecular formulas of the montmorillonite and illite are $Na_{0.75}(Si_{7.75}Al_{0.25})(Al_{3.5}Mg_{0.5})O_{20}(OH)_4$ and $K(Si_7Al)Al_4O_{20}(OH)_4$, respectively. These models of illite and montmorillonite are widely used in prior MD studies.[3, 4] The negative charge of the illite surface is larger than that of the montmorillonite surface. The initial crystal model contains substitutions, replacing Al^{3+} with Mg^{2+} in the octahedral sheets and Si^{4+} with Al^{3+} in the tetrahedral sheets, conforming to Loewenstein's rule.[5] We used 285 Na^+ and Cl^- resulting in a salinity of 3.5 wt%, which is close to real seawater.[3] A homogeneous solution containing 4424 gas molecules and 25440 water molecules was placed in montmorillonite-illite mixed clay sediments. 142 Na^+ and 512 K^+ ions were placed in the homogeneous solution to compensate for the negative charge of montmorillonite and illite, respectively. This gas-water ratio is in line with the standard SI-type hydrate, enabling the potential formation of CH_4 or CH_4/CO_2 hydrates involving all H_2O and gas molecules. To maintain charge neutrality of the edge local structures and the nanoparticles, the charge distribution of atoms on the edge surface was adjusted (see Fig. S1). In natural clay systems, particularly at the edges of clay particles, the atomic structure is often altered due to interactions with water, ions, and other molecules. This hydroxylation is used to balance the charge of the edge atoms, which could otherwise lead to unrealistic interactions with surrounding molecules. These adjustments are not expected to significantly alter the intrinsic chemical reactivity of the montmorillonite nanoparticle. Instead, they ensure that the nanoparticle behaves similarly to natural montmorillonite in hydrate-bearing sediments, where edge hydroxylation and ion adsorption are common. Two systems containing different gases (pure CH_4 or a mixture of CH_4 and CO_2) in montmorillonite-illite mixed clay sediments were tested. We refer to these two systems hereafter as $Mixed_{CH_4}$ and $Mixed_{CH_4+CO_2}$. The $Mixed_{CH_4}$ and $Mixed_{CH_4+CO_2}$ systems contained ca 13,600 and 14,500 atoms, respectively. The size of the simulation box for $Mixed_{CH_4}$ system was 82.56 Å × 125.49 Å × 127.35 Å, while the size of the simulation box for $Mixed_{CH_4+CO_2}$ system was 82.56 Å × 125.49 Å × 126.69 Å. The size of the simulation box is small, which limits the large movement of the montmorillonite nanoparticles.

S1.2 Simulation Methods

Periodic boundary conditions were assigned in all directions, and the rigidity of water molecules was preserved via the SHAKE algorithm. The Lorentz-Berthelot mixing rules[6] were used for describing the unlike interactions. For integrating the equations, the leap-frog integrator algorithm with a time step of 2.0 fs was used. All force field parameters for H_2O, CH_4, CO_2, ions, montmorillonite, and illite in the system are shown in Table S2 and Table S3. The well depth $\varepsilon_{O(CO_2)\text{-}O(H_2O)}$ between the oxygen in CO_2 and the oxygen in H_2O was scaled by a factor of 1.08. It

has been demonstrated that with such scaling, the solubility of CO_2 in water and the three-phase coexistence temperature of CO_2 hydrate can be accurately predicted.[7] Initially, the initial configurations were energy minimized by using the steepest descent algorithm. A 2-ns pre-equilibration was performed in the isothermal-isobaric (*NPT*) ensemble, with the temperature (260 K) and pressure (100 bar) controlled by velocity-rescaling thermostat[8] (time constants of 0.1 ps) and Berendsen barostat[9] (time constants of 1.0 ps), respectively. The condition of low temperature and high pressure accelerates hydrate formation and reduces computational cost.[3] Finally, a 3.0 μs production run was carried out at the *NPT* ensemble, with temperature and pressure controlled by the Nosé-Hoover thermostat[10] (time constants of 2.0 ps) and Parrinello-Rahman barostat[11] (time constants of 4.0 ps), respectively. The xy-plane of the illite layer, being infinite and rigid, would not compress significantly even under varying pressure conditions. The pressure coupling was semi-isotropic, allowing independent fluctuations along the normal (z-dimension) and lateral (xy-dimensions) directions. The F_4 order parameter[12] serves as an effective discriminator for distinguishing the water phase, with average values of -0.04, -0.4, and 0.7 for liquid water, ice, and hydrate, respectively. To monitor the formation of CH_4 and CH_4/CO_2 hydrates in montmorillonite-illite mixed clay sediments, the cage analysis algorithm proposed by Jacobson *et al.*[13] was used to display the seven cage types (5^{12}, $5^{12}6^2$, $5^{12}6^3$, $5^{12}6^4$, $4^15^{10}6^2$, $4^15^{10}6^3$, and $4^15^{10}6^4$). We apply a constant force to the atoms on the pseudo-hexagonal montmorillonite nanoparticles for the tensile, compressive, and sheer simulations. The constant pull rate is 2 Å/ns. The simulation time is 1 ns, with the trajectory is saved every 1 ps. The positions of the atoms on the left edge of the pseudohexagonal montmorillonite nanoparticles were fixed during tension, compression, and shear deformation.

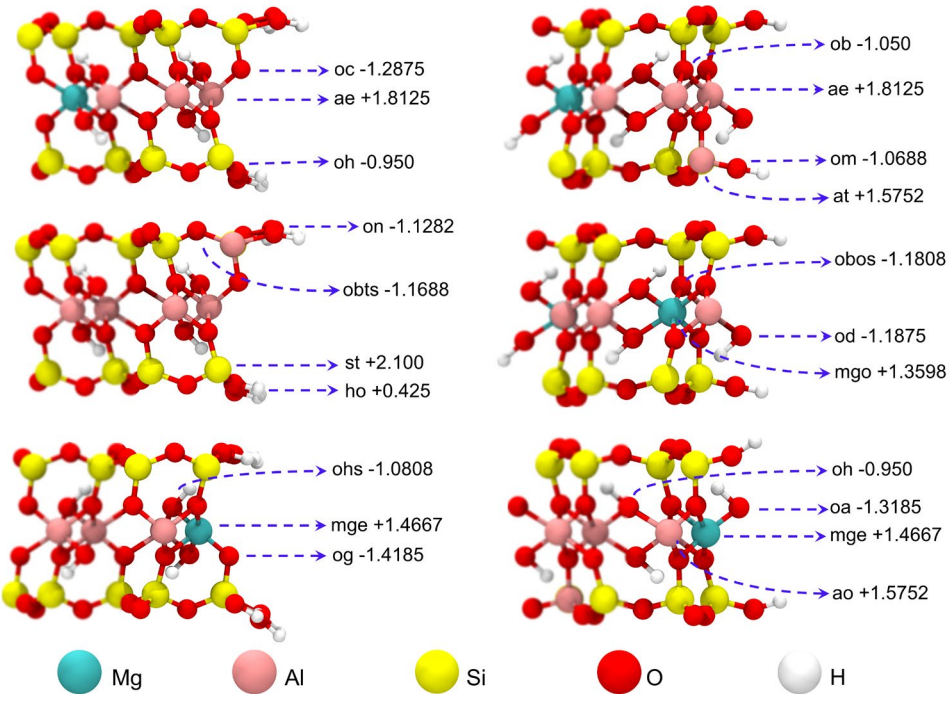

FIG. S1. Schematic illustration of the edge structure for the pseudo-hexagonal montmorillonite nanoparticles. The final charges of edge atoms for pseudo-hexagonal montmorillonite nanoparticle within our model are shown.

TABLE S1. Number of molecules of each species for the two different simulations.

	montmorillonite-illite mixed clay sediments					
System	N_{CO_2}	N_{CH_4}	N_{K^+}	N_{Na^+}	N_{Cl^-}	N_{H_2O}
$Mixed_{CH_4}$	0	4424	512	427	285	25440
$Mixed_{CH_4+CO_2}$	2212	2212	512	427	285	25440

TABLE S2. Parameters for the TIP4P/ice water model,[14] OPLS-UA CH_4,[15] and the TraPPE CO_2.[16] σ and ε are the Lennard-Jones parameters, in units of nm and kJ/mol, respectively; q is the partial charge of an atom in units of elementary charge (e); m is the atomic mass in units of g/mol.

atom	ε / [kJ/mol]	σ / [nm]	q / [e]	m / [g/mol]
H_2O				
O (MW)	0	0	-1.1794	0
O	0.8822	0.31668	0	16
H	0	0	0.5897	1.008
CH_4	1.23	0.373	0	16
CO_2				
C	0.224478	0.28	0.70	12.011
O	0.656806	0.305	-0.35	15.9994
O (OM)	0	0	0	0
Ion				
Cl	0.418998	0.439997	-1.0	35.453
Na	0.544572	0.235002	1.0	22.989
K	0.41858	0.333401	1.0	39.0983

TABLE S3. Parameters for the CLAYFF force field.[17] σ and ε are the Lennard-Jones parameters, in units of nm and kJ/mol, respectively; q is the partial charge of an atom in units of elementary charge (e); m is the atomic mass in units of g/mol.

atom	ε / [kJ/mol]	σ / [nm]	q / [e]	m / [g/mol]
Clay				
Si (st)	7.70065×10^{-6}	0.3302	2.1	28.09
Si (so)	7.70065×10^{-6}	0.3302	2.1	28.09
Mg (mgo)	3.77807×10^{-6}	0.5264	1.3598	24.31
Mg (mge)	3.77807×10^{-6}	0.5264	1.4667	24.31
Al (ao)	5.56388×10^{-6}	0.4271	1.575	26.98
Al (at)	7.70065×10^{-6}	0.3302	1.5752	26.98
Al (ae)	5.56388×10^{-6}	0.4271	1.8125	26.98
O (ob)	0.65017	0.316556	-1.05	16
O (obts)	0.65017	0.316556	-1.1688	16
O (obos)	0.65017	0.316556	-1.1808	16
O (oc)	0.65017	0.316556	-1.2875	16
O (oa)	0.65017	0.316556	-1.3185	16
O (od)	0.65017	0.316556	-1.1875	16
O (og)	0.65017	0.316556	-1.4185	16
O (om)	0.65017	0.316556	-1.0688	16
O (on)	0.65017	0.316556	-1.1282	16
O (oh)	0.65017	0.316556	-0.95	16
O (ohs)	0.65017	0.316556	-1.0808	16
H (ho)	0	0	0.425	1.008

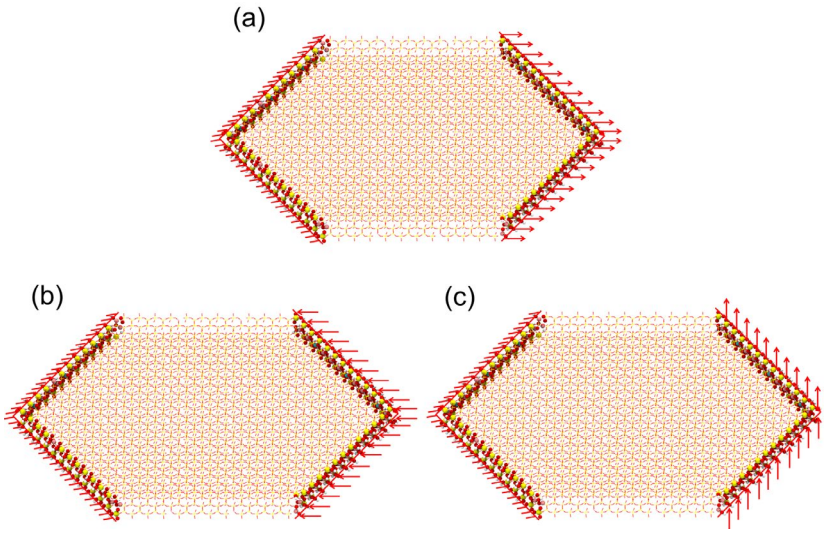

FIG. S2. Schematic illustration of mechanical (a) tensile, (b) compressive, and (c) sheer processes of pseudo-hexagonal montmorillonite nanoparticles.

S2. Calculation of properties

Gas mole fraction

We use the VMD software[18] to determine the state of gas molecules (CH_4 and CO_2 molecules) or water molecules. At each frame, we check each gas molecule to find the number of water molecules and other gas molecules surrounding it. This method is used to determine whether each gas molecule belongs to the water phase or nanobubbles. The gas mole fraction in the aqueous phase is defined as the number of gas molecules in the aqueous phase divided by the number of water and gas molecules in the aqueous phase, as follows:

$$\text{gas mole fraction} = \frac{N_{gas}}{N_{gas} + N_{water}} \quad (1)$$

Where N_{gas} is the number of gas molecules (CH_4 and CO_2 molecules) in the aqueous phase. N_{water} is the number of water molecules.

F_4 order parameter

The F_4 order parameter serves as an effective discriminator for distinguishing the water phase, with average values of -0.04, -0.4, and 0.7 for liquid water, ice, and hydrate, respectively[12]. The F_4 order parameter is defined by

$$F_4 = \langle cos(3\emptyset) \rangle \quad (2)$$

The value of F_4 is computed by the water-water pair as a function of the torsional angle $\emptyset$ between oxygen

166 atoms within 3.5 Å and the outermost hydrogen atoms in the water-water pairs.

167

168

169 **S3. Supporting Figures**

170

171

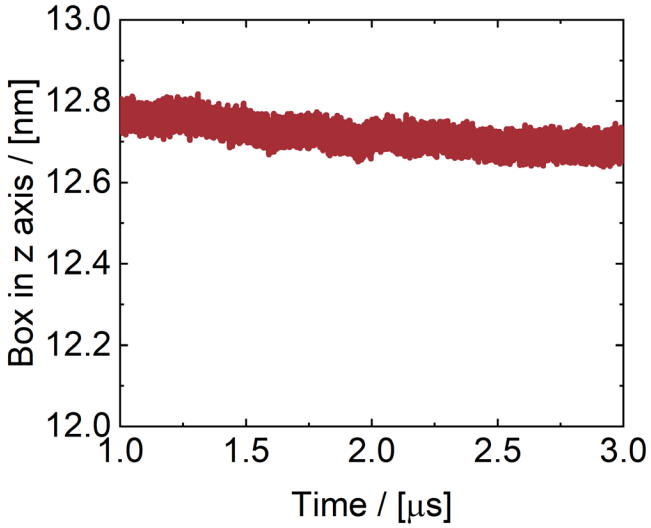

172

173 **FIG. R3.** Evolution of the box in the z-axis for the Mixed$_{CH_4}$ system.

174

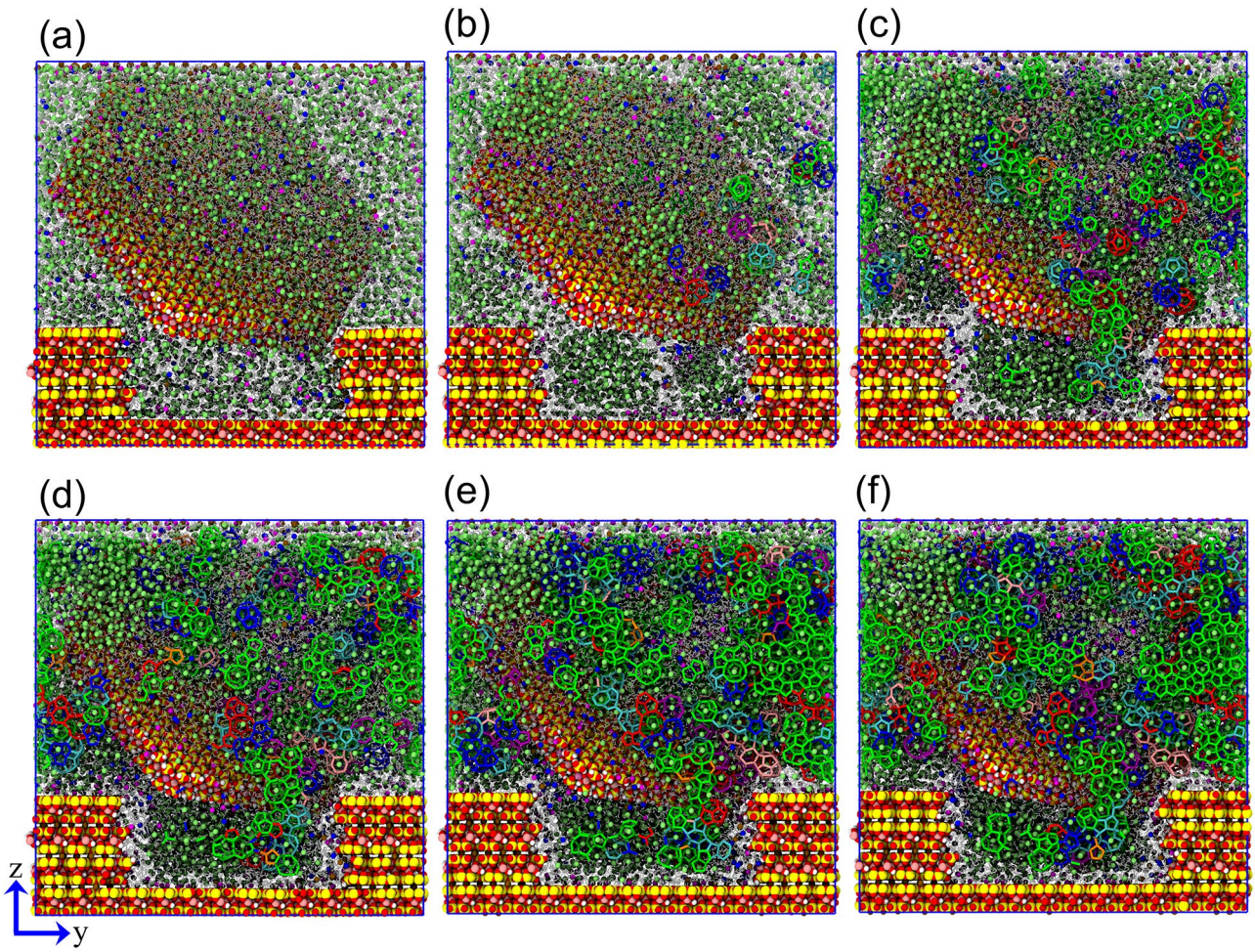

FIG. S4. (a-f) Formation processes of CH_4 hydrate in montmorillonite-illite mixed clay sediments for the $Mixed_{CH_4}$ system. Pseudo-hexagonal montmorillonite nanoparticle and illite layers are displayed as yellow (Si atom), pink (Al atom), red (O atom), and white (H atom). Green balls, blue balls, magenta balls, and silver lines represent CH_4, Na^+, Cl^-, and H_2O molecules, respectively. Hydrate cages are shown as sticks in various colors (green for 5^{12}, blue for $5^{12}6^2$, red for $5^{12}6^3$, orange for $5^{12}6^4$, cyan for $4^15^{10}6^2$, purple for $4^15^{10}6^{3,}$ and pink for $4^15^{10}6^4$).

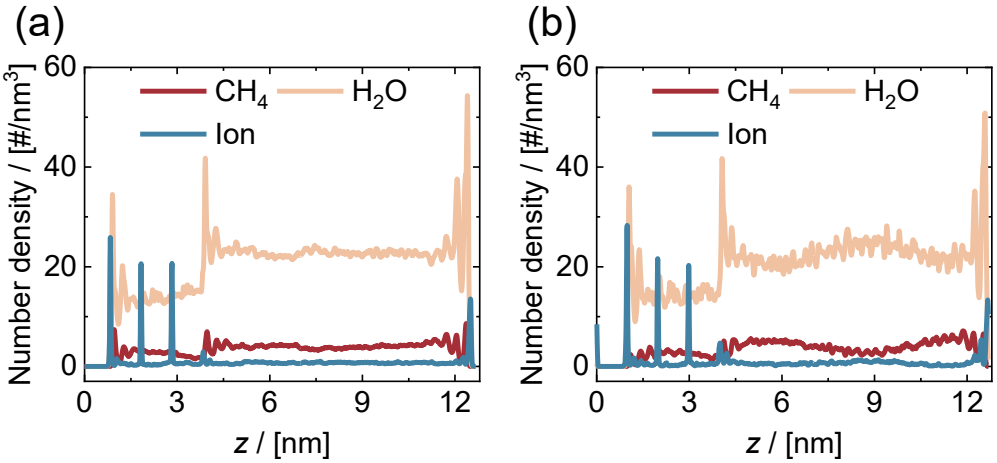

184

185 **FIG. S5.** Number density distribution of H_2O, CH_4, and ions along the surface normal direction (z-axis) (a) for
186 0.05 - 0.1 μs and (b) 2.95 - 3.0 μs in the Mixed$_{CH_4}$ system.

187

188

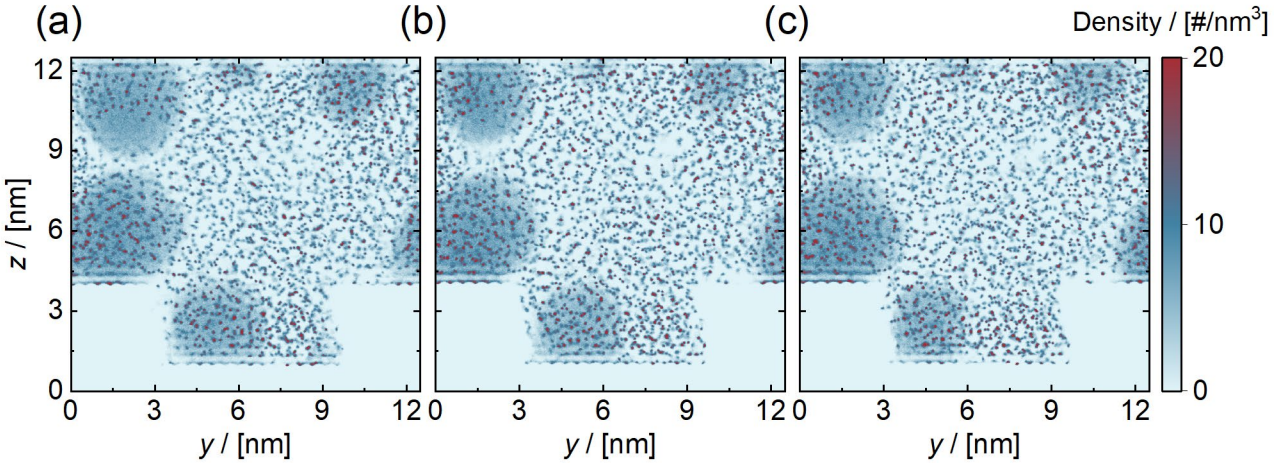

189

190 **FIG. S6.** Number density distributions of CH_4 molecules (a) for 0.95 - 1.0 μs, (b) 1.95 - 2.0 μs, and (c) 2.95 - 3.0
191 μs in the Mixed$_{CH_4}$ system.

192

193

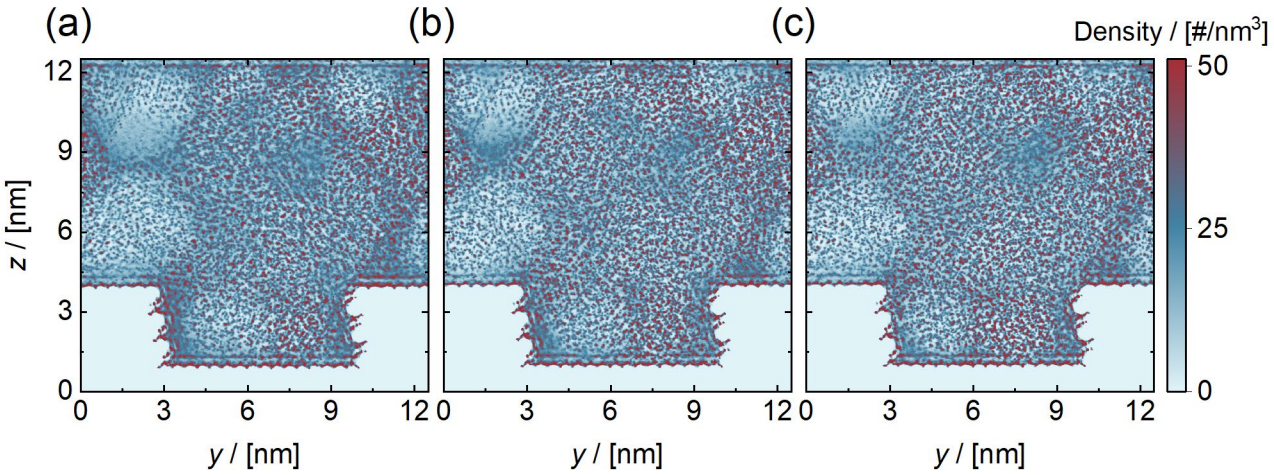

FIG. S7. Number density distributions of H_2O molecules (a) for 0.95 - 1.0 μs, (b) 1.95 - 2.0 μs, and (c) 2.95 - 3.0 μs in the $Mixed_{CH_4}$ system.

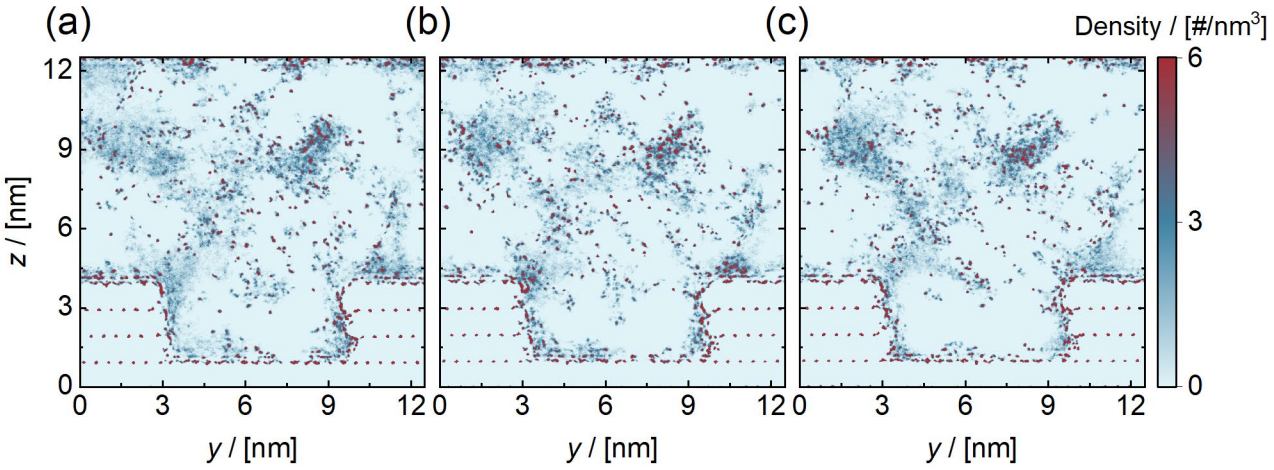

FIG. S8. Number density distributions of ions (a) for 0.95 - 1.0 μs, (b) 1.95 - 2.0 μs, and (c) 2.95 - 3.0 μs in the $Mixed_{CH_4}$ system.

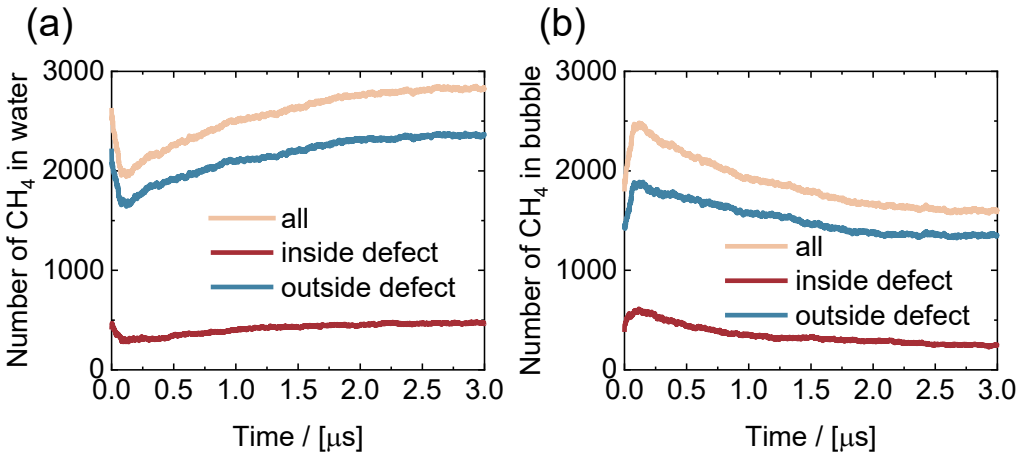

FIG. S9. Evolution of the number of CH_4 molecules (a) in the water and (b) in the nanobubbles inside and outside clay defect for the $Mixed_{CH_4}$ system.

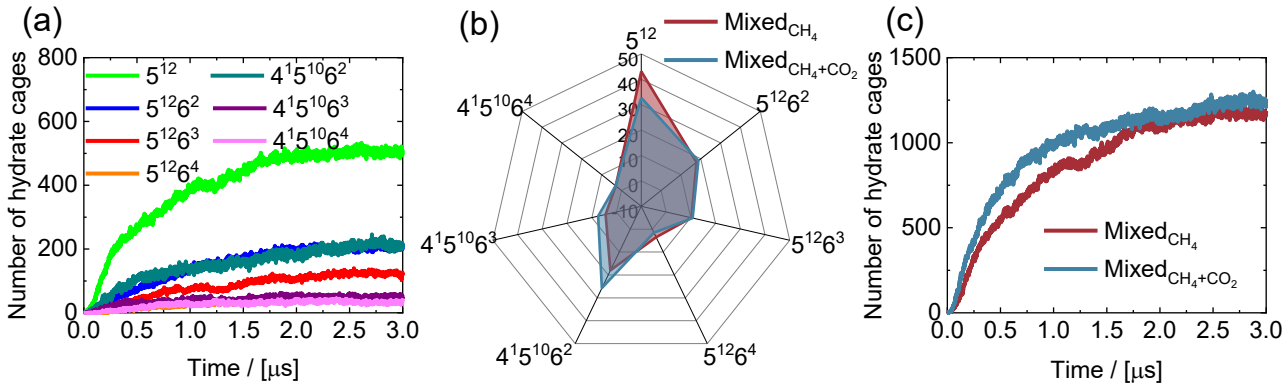

FIG. S10. Evolution of the number of (a) seven hydrate cages in the $Mixed_{CH_4}$ system and (c) total cages in the $Mixed_{CH_4}$ and $Mixed_{CH_4+CO_2}$ systems. The (b) average proportion of seven types of hydrate cages in the two systems for 2.95 - 3.0 μs.

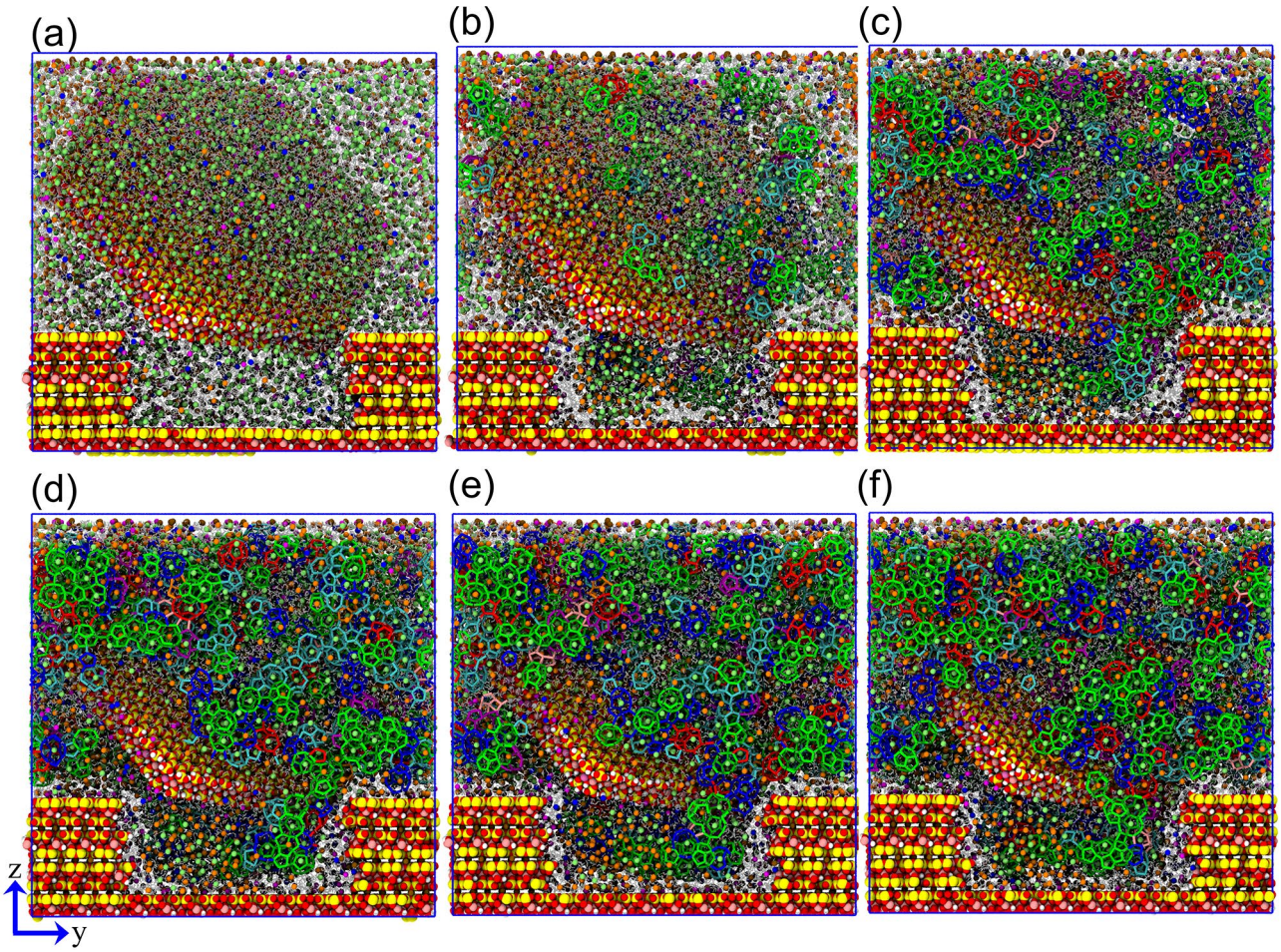

FIG. S11. (a-f) Formation processes of CH_4/CO_2 mixed hydrates in montmorillonite-illite mixed clay sediments for the $Mixed_{CH_4+CO_2}$ system. Pseudo-hexagonal montmorillonite nanoparticle and illite layers are displayed as yellow (Si atom), pink (Al atom), red (O atom), and white (H atom). Green balls, orange balls, blue balls, magenta balls, and silver lines represent CH_4, CO_2, Na^+, Cl^-, and H_2O molecules, respectively. Hydrate cages are shown as sticks in various colors (green for 5^{12}, blue for $5^{12}6^2$, red for $5^{12}6^3$, orange for $5^{12}6^4$, cyan for $4^15^{10}6^2$, purple for $4^15^{10}6^3$, and pink for $4^15^{10}6^4$).

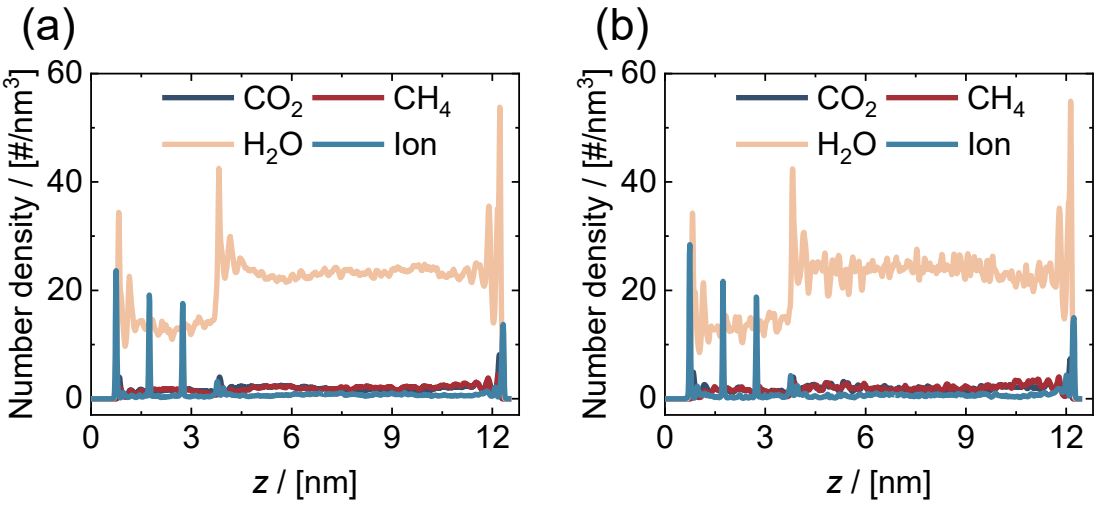

225

226 **Fig. S12.** Number density distribution of H_2O, CO_2, CH_4, and ions along the surface normal direction (z-axis) (a)
227 for 0.05 - 0.1 μs and (b) 2.95 - 3.0 μs in the Mixed$_{CH_4+CO_2}$ system.

228

229

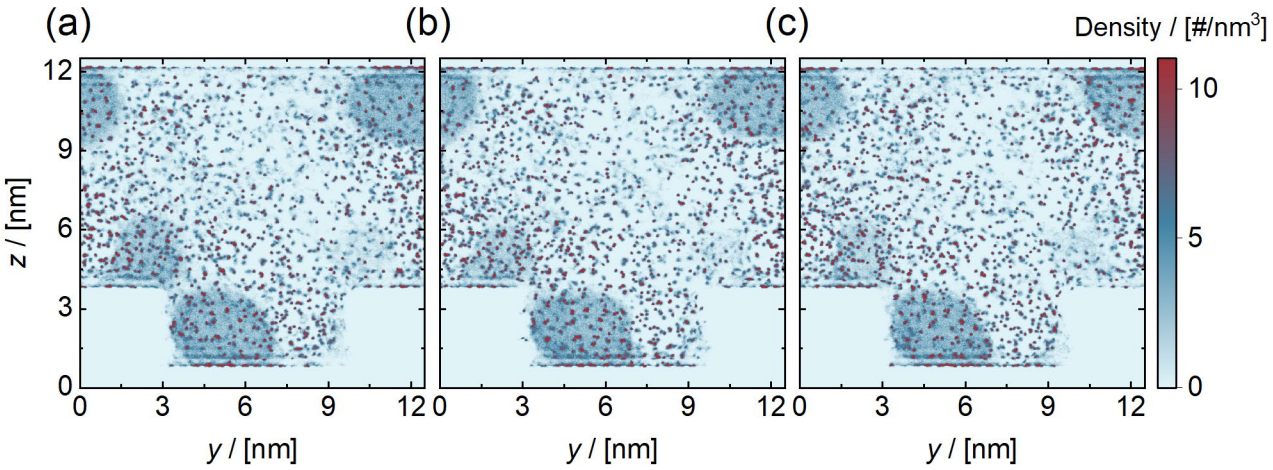

230

231 **FIG. S13.** Number density distributions of CO_2 molecules (a) for 0.95 - 1.0 μs, (b) 1.95 - 2.0 μs, and (c) 2.95 - 3.0
232 μs in the Mixed$_{CH_4+CO_2}$ system.

233

234

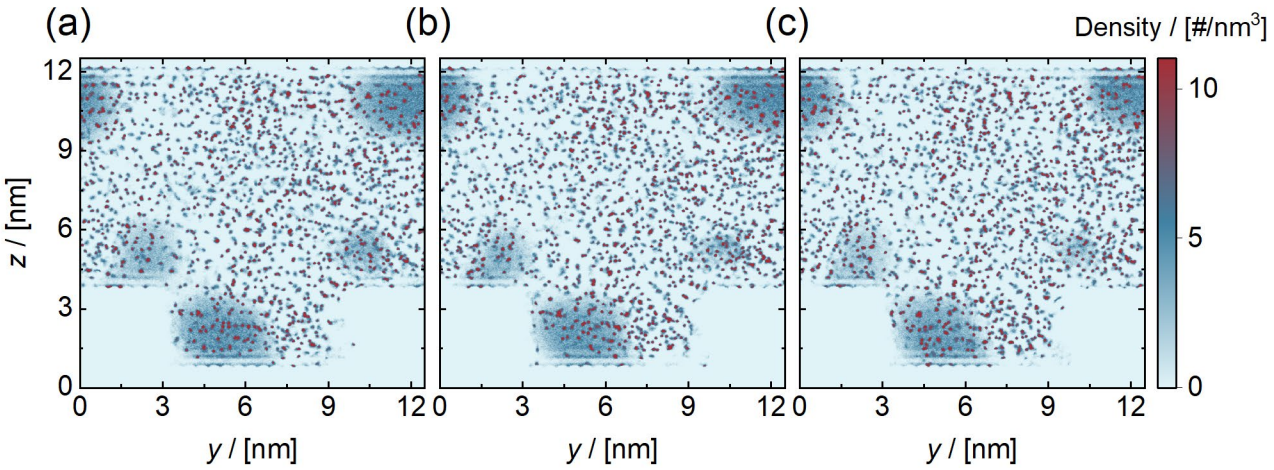

235

236 **FIG. S14.** Number density distributions of CH_4 molecules (a) for 0.95 - 1.0 μs, (b) 1.95 - 2.0 μs, and (c) 2.95 - 3.0

237 μs in the Mixed$_{CH_4+CO_2}$ system.

238

239

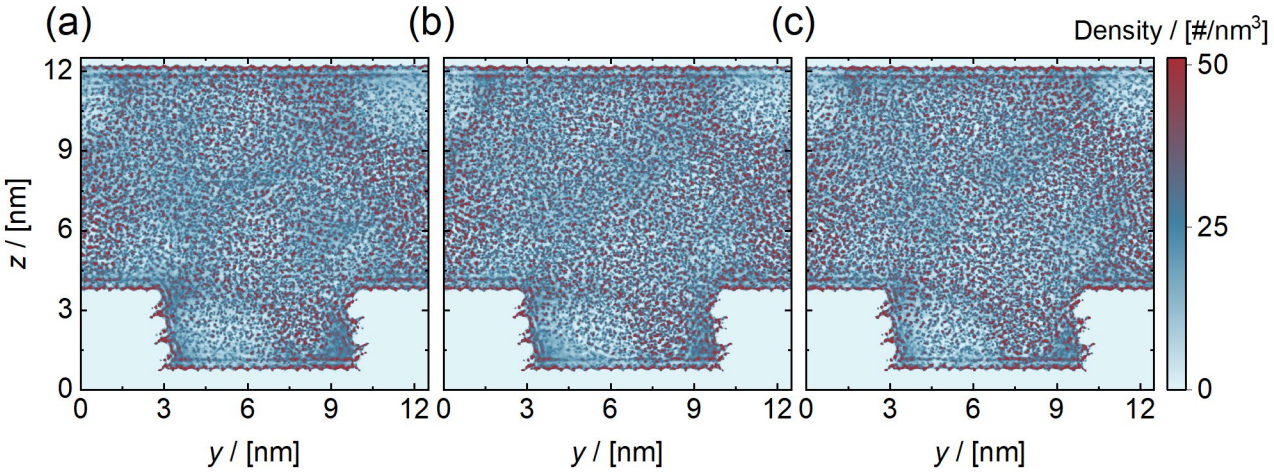

240

241 **FIG. S15.** Number density distributions of H_2O molecules (a) for 0.95 - 1.0 μs, (b) 1.95 - 2.0 μs, and (c) 2.95 - 3.0

242 μs in the Mixed$_{CH_4+CO_2}$ system.

243

244

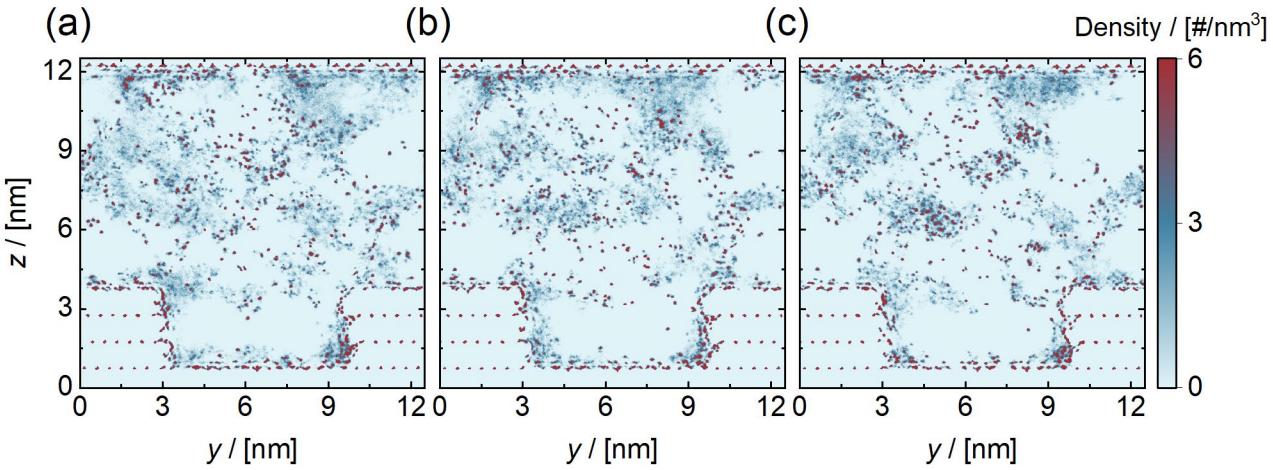

245

246 **FIG. S16.** Number density distributions of ions (a) for 0.95 - 1.0 μs, (b) 1.95 - 2.0 μs, and (c) 2.95 - 3.0 μs in the
247 Mixed$_{CH_4+CO_2}$ system.

248

249

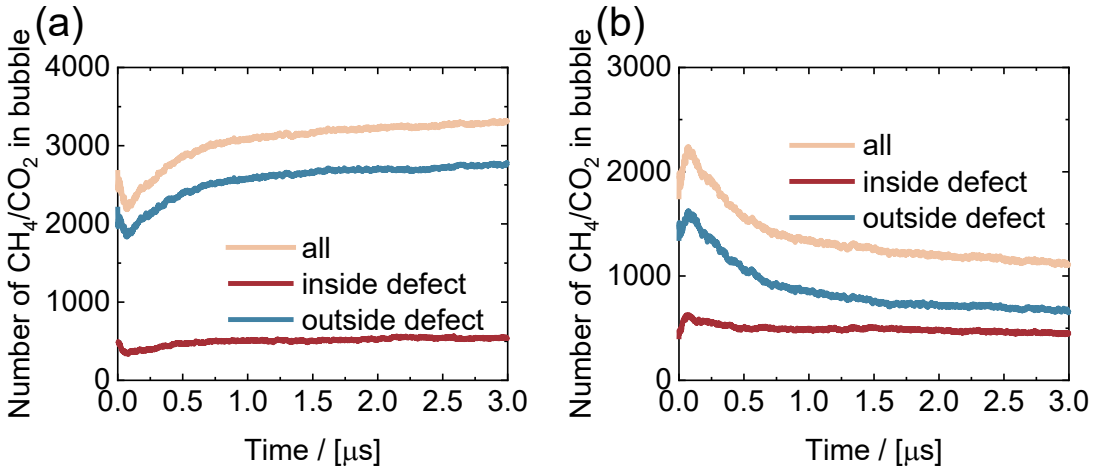

250

251 **FIG. S17.** Evolution of the number of CH_4/CO_2 molecules (a) in the water and (b) in the nanobubbles inside and
252 outside the clay defect for the Mixed$_{CH_4+CO_2}$ system.

253

254

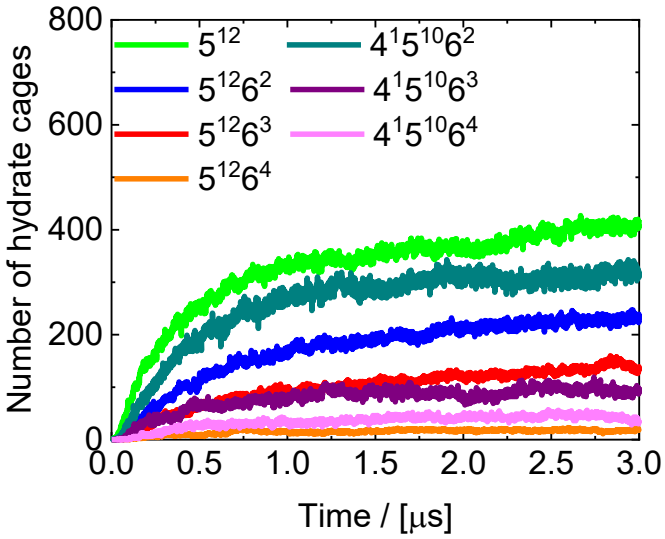

FIG. S18. Evolution of the number of hydrate cages in the $Mixed_{CH_4+CO_2}$ system.

S4. Supporting Videos

VIDEO S1. Formation process of CH_4 hydrates in the montmorillonite-illite mixed clay sediments for the $Mixed_{CH_4}$ system. Pseudo-hexagonal montmorillonite nanoparticle and illite layers are displayed as yellow (Si atom), pink (Al atom), red (O atom), and white (H atom). Green balls represent CH_4 molecules. Hydrate cages are shown as sticks in various colors (green for 5^{12}, blue for $5^{12}6^2$, red for $5^{12}6^3$, orange for $5^{12}6^4$, cyan for $4^15^{10}6^2$, purple for $4^15^{10}6^3$, and pink for $4^15^{10}6^4$).

VIDEO S2. Formation process of CH_4/CO_2 mixed hydrates in the montmorillonite-illite mixed clay sediments for the $Mixed_{CH_4+CO_2}$ system. Pseudo-hexagonal montmorillonite nanoparticle and illite layers are displayed as yellow (Si atom), pink (Al atom), red (O atom), and white (H atom). Green balls, orange balls, and silver lines represent CH_4, CO_2, and H_2O molecules, respectively. Hydrate cages are shown as sticks in various colors (green for 5^{12}, blue for $5^{12}6^2$, red for $5^{12}6^3$, orange for $5^{12}6^4$, cyan for $4^15^{10}6^2$, purple for $4^15^{10}6^3$, and pink for $4^15^{10}6^4$).

S5. Supporting files

FILE S1. Initial configuration for the $Mixed_{CH_4}$ system.

FILE S2. Initial configuration for the $Mixed_{CH_4+CO_2}$ system.

References

[1] J. F. Li, J. L. Ye, X. W. Qin, H. J. Qiu, N. Y. Wu, H. L. Lu, W. W. Xie, J. A. Lu, F. Peng, Z. Q. Xu *et al.*, "The first offshore natural gas hydrate production test in South China Sea," China Geology **1,** 5 (2018).

[2] R. T. Downs, and M. Hall-Wallace, "The crystal structure database," Am. Mineral. **88,** 247 (2003).

[3] F. Mi, Z. He, G. Jiang, and F. Ning, "Effects of marine environments on methane hydrate formation in clay nanopores: A molecular dynamics study," Science of the Total Environment **852,** 158454 (2022).

[4] Y. Li, M. Chen, H. Tang, S. B. Han, H. Z. Song, P. F. Wang, Y. S. Zhao, and J. L. Zhu, "Insights into Carbon Dioxide Hydrate Nucleation on the External Basal Surface of Clay Minerals from Molecular Dynamics Simulations," ACS Sustain. Chem. Eng. **10,** 6358 (2022).

[5] W. Loewenstein, "The Distribution of Aluminum in the Tetrahedra of Silicates and Aluminates," Am. Mineral. **39,** 92 (1954).

[6] M. P. Allen, and D. J. Tildesley, *Computer simulation of liquids* (Oxford university press, 2017), 2nd edn.

[7] J. Costandy, V. K. Michalis, I. N. Tsimpanogiannis, A. K. Stubos, and I. G. Economou, "The role of intermolecular interactions in the prediction of the phase equilibria of carbon dioxide hydrates," J Chem Phys **143,** 094506 (2015).

[8] G. Bussi, D. Donadio, and M. Parrinello, "Canonical sampling through velocity rescaling," J Chem Phys **126,** 014101 (2007).

[9] H. J. C. Berendsen, J. P. M. Postma, W. F. Vangunsteren, A. Dinola, and J. R. Haak, "Molecular-Dynamics with Coupling To an External Bath," J. Chem. Phys. **81,** 3684 (1984).

[10] S. Nosé, "A Molecular-Dynamics Method for Simulations in the Canonical Ensemble," Mol. Phys. **52,** 255 (1984).

[11] M. Parrinello, and A. Rahman, "Crystal-Structure and Pair Potentials - a Molecular-Dynamics Study," Phys. Rev. Lett. **45,** 1196 (1980).

[12] L. A. Báez, and P. Clancy, "Computer Simulation of the Crystal Growth and Dissolution of Natural Gas Hydrates a," Ann. N.Y. Acad. Sci. **715,** 177 (1994).

[13] L. C. Jacobson, W. Hujo, and V. Molinero, "Thermodynamic stability and growth of guest-free clathrate hydrates: a low-density crystal phase of water," J. Phys. Chem. B **113,** 10298 (2009).

[14] J. L. Abascal, E. Sanz, R. Garcia Fernandez, and C. Vega, "A potential model for the study of ices and amorphous water: TIP4P/Ice," J. Chem. Phys. **122,** 234511 (2005).

[15] W. L. Jorgensen, J. D. Madura, and C. J. Swenson, "Optimized Intermolecular Potential Functions for Liquid Hydrocarbons," J. Am. Chem. Soc. **106,** 6638 (1984).

[16] J. J. Potoff, and J. I. Siepmann, "Vapor–liquid equilibria of mixtures containing alkanes, carbon dioxide, and nitrogen," AlChE J. **47,** 1676 (2001).

[17] R. T. Cygan, J. J. Liang, and A. G. Kalinichev, "Molecular models of hydroxide, oxyhydroxide, and clay phases and the development of a general force field," J. Phys. Chem. B **108,** 1255 (2004).

[18] W. Humphrey, A. Dalke, and K. Schulten, "VMD: visual molecular dynamics," J Mol Graph **14,** 33 (1996).

314